Efficient Methods for Aircraft Frequency Response Estimation at NASA ⋆

Jared A. Grauer *

* *NASA Langley Research Center, Hampton, VA 23681 USA (e-mail: jared.a.grauer@nasa.gov).*

Abstract: Methods developed at NASA for efficiently estimating multiple-input multiple-output frequency responses of various aircraft control loops are discussed. These methods use simultaneous orthogonal multisine excitations and ratios of input-output Fourier transform data that can be computed in real time. An example is given to demonstrate some of the methods using flight test data for the X-56A airplane.

Keywords: Frequency responses, Multisine inputs, Aircraft system identification, Real time.

1. INTRODUCTION

Aircraft system identification is the process of identifying mathematical models of an aircraft and its components from measured data. One common goal of a system identification analysis is to estimate parametric models of the aerodynamic forces and moments acting on the aircraft involving stability and control derivatives.

NASA has a long history in aircraft system identification, as summarized by Morelli and Klein (2005), beginning in 1919 as the NACA Langley Memorial Aeronautical Laboratory. Over the last century, new flight test and analysis techniques have been continually developed, tested, and refined at NASA. Many of the techniques currently used are presented by Morelli and Klein (2016), with the MATLAB®-based software called System IDentification Programs for AirCraft, or SIDPAC, available through the NASA Software Catalog by Morelli (2002).

Of the many system identification techniques, frequency response modeling has some advantages and is commonly used. In addition to aerodynamic modeling, Tischler and Remple (2012) mentions other applications of frequency response modeling such as handling qualities specification compliance, disturbance rejection bandwidth determination, reduced-order modeling of complicated simulations, stability-margin testing, and control law validation. Furthermore, modeling in the frequency domain gives physical insight, lowers computational demands, and has other practical advantages. See Tischler and Remple (2012), Morelli and Klein (2016), and Morelli and Grauer (2020) for more discussion.

In a typical flight test, the pilot captures a flight condition and performs a series of maneuvers. This process is then repeated for other test points in the flight envelope, which are typically parameterized in terms of speed or Mach number, altitude, and weight. Analyzing about 200 flight conditions is common for standard fighter aircraft. As discussed in Tischler and Remple (2012), conventional maneuvers using frequency sweeps are applied to individual inputs. Additional maneuvers are needed to apply frequency sweeps to other inputs. This can require a large amount of time and money to perform a flight test campaign. This problem is compounded for modern aircraft configurations having numerous control effectors, such as advanced fighters, urban air mobility vehicles, or aeroelastic aircraft.

To address this reoccurring and growing problem, techniques have been developed at NASA to efficiently conduct flight tests and system identification analyses using frequency responses. The approach involves applying orthogonal multisine excitations to multiple inputs at the same time and estimating frequency responses using ratios of Fourier transform data. This enables the simultaneous estimation of many different frequency responses from a single maneuver, thereby saving time and money. Furthermore, the matching between the experiment and the theory facilitates relatively simple computations for the frequency response estimates, which can be done in real time without engineering judgment of the analyst. These techniques have been used at NASA and other institutions to reduce time and costs for flight tests, wind tunnel tests, and obtaining reduced-order models of complicated simulations.

This paper summarizes efficient methods for frequency response estimation developed at NASA and demonstrates applications using flight test data. Section 2 reviews theoretical background. Section 3 summarizes past approaches for frequency response estimation. This provides context for Section 4, which presents the current, efficient methods. Section 5 demonstrates several applications using the X-56A airplane. Section 6 concludes the paper.

2. THEORETICAL BACKGROUND

For a linear time-invariant system, the frequency response $G(j\omega)$ quantifies the relative amplification and phase shift of the steady-state response due to a sinusoidal input. Given the steady-state input and output

$$u(t) = a\sin(\omega t + \phi), \qquad y(t) = b\sin(\omega t + \psi) \tag{1}$$

⋆ This research was supported by NASA under the Advanced Air Transport Technology (AATT) project.

the associated frequency response is defined as

$$G(j\omega) = \left|\frac{b}{a}\right| e^{j(\psi-\phi)} = \frac{y(j\omega)}{u(j\omega)} \tag{2}$$

As such, frequency responses are complex valued and can be described in terms of their real and imaginary parts, or in terms of their magnitude and phase angle given in units of dB and deg, respectively.

Frequency responses are commonly used in aircraft flight dynamics because they are fundamental analysis tools that provide physical insight into the system and are used to quantify design specifications.

3. PAST APPROACHES FOR FREQUENCY RESPONSE ESTIMATION

Aircraft frequency responses were first estimated from flight test data by Milliken (1947). An input was sinusoidally moved until the steady-state response developed, from which the relative amplitude and phase could be determined per the first equality in Eq. (2). This lengthy process was then repeated for additional frequencies, inputs, and flight conditions.

Later, Seamans et al. (1950) used shorter pulse inputs and ratios of Fourier transforms to compute frequency responses, per the second equality in Eq. (2). However, the estimates were inaccurate due to transient responses in the data, short record durations, and low input power.

Advances in numerical analysis made frequency response estimation based on spectral densities, discussed in Bendat and Piersol (1986), standard practice. These are typically applied using frequency sweep inputs to provide continuous input power within a bandwidth of interest. More details and advanced techniques for this are discussed in Tischler and Remple (2012). The basic techniques, employing the fast Fourier transform (FFT), were applied during the flight testing of the X-29A airplane by Bosworth and West (1986) and enabled quasi-real-time comparison of stability margins against pre-flight predictions and facilitated a faster expansion of the flight envelope.

Bosworth and Burken (1997) applied Schroeder sweeps to multiple inputs of the X-31A nonlinear simulation to compute a multiple-input multiple-output (MIMO) transfer function matrix and extract multivariable stability margins. This approach was also applied to the X-38 nonlinear simulation by Bosworth and Stachowiak (2005) using a recursive Fourier transform to enable real-time estimation for an efficient Monte Carlo analysis. Similar analyses were conducted on the X-43A flight data by Baumann (2007), the X-48B flight data by Regan (2008), and the ARES I-X nonlinear simulation by Brandon et al. (2008). In Holzel and Morelli (2011), a real-time estimate of the frequency response was obtained using multisine inputs and a recursive Fourier transform based on least-squares fits to time-domain data.

4. CURRENT EFFICIENT APPROACHES FOR FREQUENCY RESPONSE ESTIMATION

Figure 1 shows a simplified block diagram for a modern aircraft system. The pilot primarily interacts with the system using the stick and pedal inceptors. These signals and sensor measurements are input to the flight control system (FCS), which generates desired forces and moments to be imparted on the aircraft. The mixer then allocates those signals to the available effectors (Act.), which are moved to the desired positions by the actuators. The bare-airframe dynamics (AC) then produce motions in the aircraft, which are observed by the sensors (Sens.).

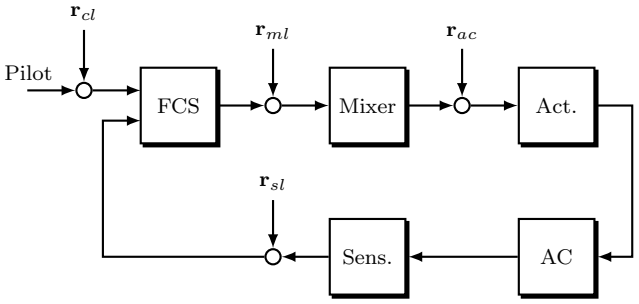

Fig. 1. Block diagram of a modern flight control system.

As mentioned before, aircraft system identification can target many of the blocks and loops shown in Fig. 1, for example open-loop or closed-loop dynamics, or the bare-airframe model parameters. To provide sufficient information for the estimation, excitation inputs (labeled as $\mathbf{r}$ in Fig. 1) are added at several points in the system.

The excitations are described next in Section 4.1. Frequency responses are estimated using the methods described in Sections 4.2 through 4.5. Fitting parametric models to frequency response data are discussed in Section 4.6.

4.1 Orthogonal Phase-Optimized Multisine Excitations

The multisines summarized here are explained in detail by Morelli and Klein (2016) and the many references therein. Each multisine is of the form

$$r_j(t) = a_j \sum_{k\in K_j} \sqrt{\Phi_k} \sin\left(\frac{2\pi k}{T}t + \phi_k\right) \tag{3}$$

for $j = 1, 2, \ldots, n_r$ and sets K_j. The excitation time duration T, which determines the fundamental frequency and the frequency resolution $1/T$ Hz, is selected first, based on constraints for the flight test and analysis.

The available (discrete) excitation frequencies are $\omega_k = 2\pi k/T$ where the integers k are harmonics. These frequencies are selected to span a bandwidth of interest. For multiple inputs, the harmonics are uniquely distributed to different multisines, which can be done because harmonic sinusoids are mutually orthogonal over T.

The normalized power spectrum Φ_k is then designed for each multisine. Often this is constant over frequency; however, it can be shaped to emphasize or de-emphasize specific bandwidths.

Afterwards, a numerical optimization is performed to determine the phase angle spectrum ϕ_k for each multisine that minimizes the relative peak factor (RPF). This optimization creates inputs with low peak-to-peak amplitudes in the responses, which helps create good responses for linear modeling. The multisines are then shifted in time

until they start and end at zero, to provide a perturbation input.

Lastly, the overall gains a_j are designed for each multisine. This is usually done to achieve good signal-to-noise ratios while remaining in the linear modeling regime.

Figure 2 shows an example multisine design from Morelli (2012) used for aerodynamic modeling of the NASA T-2 airplane. A $T = 10$ s excitation was designed for the elevator δ_e, aileron δ_a, and rudder δ_r, spanning 0.2–2.2 Hz.

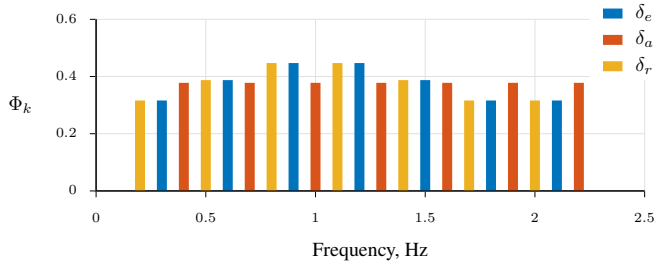

(a) Normalized power spectra.

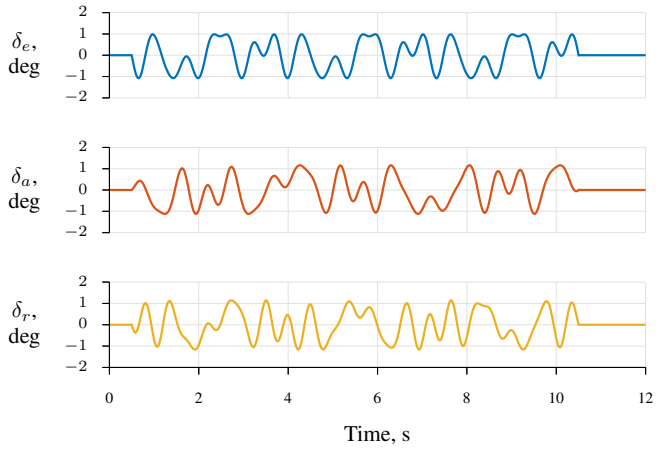

(b) Time histories.

Fig. 2. Multisine design example for the NASA T-2 aerodynamics identification, adapted from Morelli (2012).

Construction of a set of multisines is automated in the SIDPAC function `mkmsswp.m`. As discussed in Morelli and Klein (2016), these inputs have enabled efficient and accurate system identification in a variety of applications and flight conditions. The primary benefits of using multisines for the current work is that multiple inputs can be applied simultaneously, and simple procedures can be used for estimating the frequency responses, as discussed next.

4.2 Direct Method for Frequency Response Estimation

To compute frequency responses, measured input-output data from an experiment are first transformed into the frequency domain. A simple approach for this is to use the Euler approximation to the Fourier integral

$$\mathbf{z}(j\omega_k) = \Delta t \sum_{i=1}^{N} \mathbf{z}(t_i)\, e^{-j\omega_k t_i} \tag{4}$$

where the generic vector signal $\mathbf{z}$ can stand for either the input or the output, and where Δt is the sampling period, t_i is the discrete time value, and N is the number of time-domain samples.

Equation (4) is a good approximation for low frequencies relative to the Nyquist frequency. The chirp z-transform can be used for improved accuracy. This is implemented in the SIDPAC function `fint.m` with an option to use cubic spline interpolation for further improvements in accuracy.

Given Fourier transforms of the input and output data, the MIMO frequency response matrix $\hat{\mathbf{G}}(j\omega_k)$ can be assembled from the individual estimates using the direct approach, for $k \in K_j$, as

$$\hat{G}_{ij}(j\omega_k) = \frac{y_i(j\omega_k)}{u_j(j\omega_k)} \tag{5}$$

Equation (5) is similar to Eq. (2) except that is only computed at the discrete harmonic frequencies for the respective inputs. This is because for a linear system, the output steady-state response only has power at the frequencies in the input. This fact also results in a relatively small number of data points in the frequency domain, which lowers the computational burden. However, these few points have excellent signal-to-noise ratios by design. Furthermore, computing frequency responses in this way does not require the analyst to adjust any tuning parameters, such as are needed to estimate spectral density functions.

In general, Eq. (5) is an unbiased estimate of the frequency response, having a variance that is inversely proportional to the squared signal-to-noise ratio for steady-state output data over integer numbers of cycles (Ljung (1999)). Gaussian noise on the output measurements creates a proportional Gaussian distribution in the real and imaginary parts of the frequency response, as shown in Grauer (2018). Nonlinearities, unmodeled inputs, time-varying dynamics, and transient responses degrade the accuracy of frequency response estimates.

The direct approach is useful for computing frequency responses for open-loop systems — either systems without feedback or loops opened one-at-a-time with all other loops remaining closed. This approach was presented in Grauer and Morelli (2014). Estimation of frequency responses for open-loop systems from closed-loop data is discussed next.

4.3 Joint Input-Output Method for Frequency Response Estimation

When the open-loop bare-airframe frequency responses are to be identified from data involving a feedback control law or a mixer, the inputs are correlated in frequency and estimates based on the direct approach neglect important couplings, as discussed in Berger et al. (2018) and Grauer and Boucher (2020b). As a result, Berger et al. (2018) proposed using the joint input-output (JIO) method for computing frequency responses.

As outlined by Ljung (1999), under specific conditions the JIO estimate for a frequency response matrix is

$$\hat{\mathbf{G}}(j\omega_k) = \frac{\mathbf{y}(j\omega_k)}{\mathbf{u}(j\omega_k)} = \left[\frac{\mathbf{y}(j\omega_k)}{\mathbf{r}(j\omega_k)}\right]\left[\frac{\mathbf{u}(j\omega_k)}{\mathbf{r}(j\omega_k)}\right]^{-1} \tag{6}$$

Equation (6) requires the direct estimates of two frequency response matrices: the excitation to the system output

and the excitation to the system input. In order to invert the latter, per Eq. (6), there must be the same number of excitations as system inputs so that the resulting frequency response matrix is square.

The JIO approach can be applied to multiple-input data using multisine inputs. As suggested by Berger et al. (2018) and demonstrated in Grauer (2022), linear interpolation between harmonic frequencies is often sufficient for obtaining the $\mathbf{u}/\mathbf{r}$ frequency response.

The JIO approach requires additional computations and is more sensitive to the effects of errors than the direct approach due to added complexity. However, when using multisine inputs and computing frequency responses as described in Section 4.2, the additional computational burden is small. Also, because interpolation is used, the multisines must be designed with a frequency resolution fine enough to capture any lightly-damped resonances, as discussed in Grauer and Boucher (2020b).

4.4 Multiple-Loop Estimation

In Sections 4.2 and 4.3, the estimation of MIMO frequency responses for a single loop was addressed. These techniques provide considerable improvements in efficiency over conventional single-input tests for that information. Further improvements in efficiency can be realized by injecting orthogonal multisines at different points in the system and using the appropriate input-output data and estimation method to simultaneously identify frequency responses for multiple loops. In this way, MIMO frequency responses for several control loops can be identified from a single maneuver using a well-designed set of multisine inputs.

In Grauer (2022), this was demonstrated for estimating bare-airframe, closed-loop, and broken-loop (opened at the mixer inputs and the sensor outputs) frequency responses using simulation data. This was also demonstrated for estimating the same broken-loop frequency responses using flight test data.

When many MIMO loops are to be estimated simultaneously, many harmonics are needed and therefore also longer time durations. There is a tradeoff between how long a maneuver lasts and how many loops and inputs can be identified at once.

4.5 Real-Time Estimation

The discussion so far has pertained to batch estimation, after all the data for a maneuver have been collected. These techniques can also be applied in real time as data are collected.

Real-time estimation is facilitated, in part, by the recursive Fourier transform. By expanding the summation in Eq. (4) and grouping terms, as discussed by Morelli and Klein (2016) and references therein, the transform up to an arbitrary time t_i for the excitation frequencies can be written recursively as

$$\mathbf{z}_i(j\omega_k) = \mathbf{z}_{i-1}(j\omega_k) + \Delta t\, \mathbf{z}(t_i)\, e^{-j\omega_k t_i} \tag{7}$$

Using the current Fourier transform data for the inputs and outputs, frequency response estimates can then be updated per Eq. (5) or (6).

Computations for the recursive Fourier transform and the frequency responses are relatively small in burden, requiring a small number of additions and multiplications. Furthermore, they are performed only at the relatively few number of excitation frequencies in the inputs. As such, it is practical to do these calculations in real time to monitor the flight test.

These approaches have been used in several flight tests and wind tunnel tests for applications including stability margin monitoring, fault detection, and real-time dynamic modeling.

4.6 Maximum-Likelihood Parameter Estimation

It is often useful to fit dynamic models, either based on transfer functions or state-space representations, to estimated frequency responses. Some applications discussed in Tischler and Remple (2012) and Morelli and Klein (2016) include estimating stability and control derivatives for the bare-airframe dynamics to model the aerodynamic forces and moments on the vehicle or identifying low-order equivalent system models of closed-loop dynamics for handling qualities analyses.

Although this is routinely done by fitting model frequency responses to data arranged as a Bode plot, with a weighting applied to balance magnitude and phase angle errors, there are theoretical advantages to applying a maximum-likelihood estimator directly to the complex-valued frequency responses.

As discussed in Morelli and Klein (2016), Grauer (2018), and Grauer and Boucher (2020a), the relevant cost function to be minimized is

$$J = n_f \sum_{k \in K} \mathbf{v}^{\dagger}(j\omega_k)\mathbf{S}_{vv}^{-1}\mathbf{v}(j\omega_k) + n_f \log|\mathbf{S}_{vv}| \tag{8}$$

where n_f is the number of frequencies, K is the union of all sets K_j,

$$\mathbf{v}(j\omega_k) = \text{vec}\left[\hat{\mathbf{G}}(j\omega_k)\right] - \text{vec}\left[\hat{\mathbf{G}}(j\omega_k, \boldsymbol{\theta})\right] \tag{9}$$

are the modeling residuals, and $\mathbf{S}_{vv}$ is the covariance matrix for the residuals. Equation (8) derives from the negative log of the likelihood function for this estimation problem.

The goal of the optimization is to determine a vector of unknown parameters $\boldsymbol{\theta}$ that best match the model frequency responses $\hat{\mathbf{G}}(j\omega_k, \boldsymbol{\theta})$ to the frequency response data $\hat{\mathbf{G}}(j\omega_k)$. This is performed using a Gauss-Newton optimization with a relaxation technique in which $\boldsymbol{\theta}$ and $\mathbf{S}_{vv}$ are alternately optimized until both converge. This procedure is performed with a modified version of the SIDPAC function `fdoe.m`.

5. X-56A FLIGHT TEST EXAMPLES

5.1 Aircraft Description

The X-56A Multi-Utility Technology Testbed (MUTT) was built as a subsonic aeroelastic demonstrator by Lockheed Martin Aeronautics (LM Aero) for the Air Force Research Laboratory (AFRL). In 2014, the aircraft was transferred to NASA Armstrong Flight Research Center

(AFRC), where it was flown until 2019. The aircraft is unique in that it had a flutter instability purposefully designed into its normal flight envelope to facilitate modeling and control for aeroelastic aircraft. See Ryan et al. (2014) for more details about the NASA effort.

Figure 3 shows the X-56A in flight over AFRC. The aircraft has an 8.4 m wingspan and weighs between 1,780–2,220 N depending on fuel and water ballast. There are two turbojet engines and ten independent control surfaces along the trailing edges of the wings and center body. The airplane was fully instrumented for servoaeroelastic flight research with research-quality sensors.

Fig. 3. X-56A airplane (credit: NASA / Jim Ross).

Pilots flew the X-56A remotely from a mobile ground station using conventional inceptors while watching an out-the-nose video stream overlaid with a heads-up display and digital cockpit instrumentation. Flight test engineers monitored real-time displays of telemetered data. The maneuvers discussed in this section were performed by capturing a flight condition, selecting the appropriate set of multisine inputs, applying the multisines, and measuring the inputs and outputs.

5.2 Real-Time Stability Margin Monitoring

During the envelope expansion flights, stability margins were monitored and compared to pre-flight predictions. This process helped ensure the safety of flight as the flight envelope was expanded towards the flutter instability.

Multisine inputs were injected at the mixer inputs ($\mathbf{r}_{ml}$ in Fig. 1) in the roll, pitch, or yaw channels using the flight control system. The real-time estimates were then computed onboard the aircraft and telemetered to the ground station for display and comparison with pre-flight models.

Figure 4 shows a real-time estimate of the broken-loop roll frequency response, opened at the mixer. This image is a screenshot taken from the control room at NASA AFRC during Flight 8 with a classical take-off and landing control law. The solid blue lines are the pre-flight predictions, whereas the black triangles are the real-time estimates. These two plots agreed closely and enabled rapid progression through this part of the flight envelope.

5.3 Multiple-Loop Stability Margins

Also during the envelope expansion flights, other sets of multisines were used to evaluate multiple broken-loop

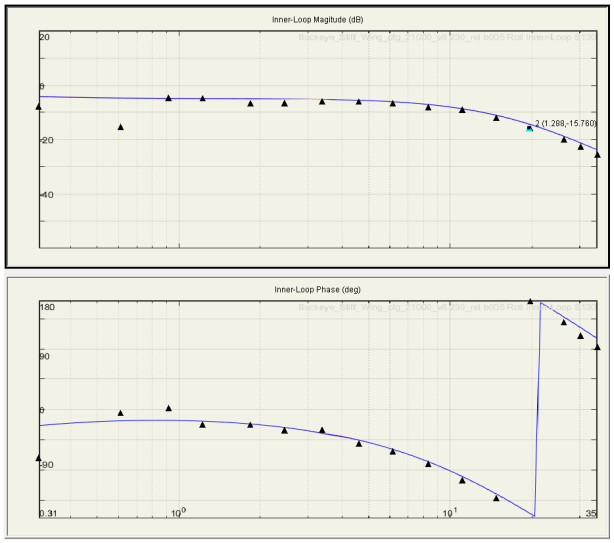

Fig. 4. X-56A real-time frequency response estimates (image courtesy of Matthew Boucher, NASA AFRC).

frequency responses at the same time. In Fig. 1, these multisines were for $\mathbf{r}_{ml}$ and $\mathbf{r}_{sl}$.

Figure 5 shows the estimated longitudinal broken-loop frequency responses, opened at both the elevator mixer input and the pitch rate sensor output, from Flight 15. Numbers have been removed because these data are ITAR-restricted. Although the elevator loop had low signal-to-noise for about the higher third of frequencies, these data were useful in verifying the longitudinal stability margins.

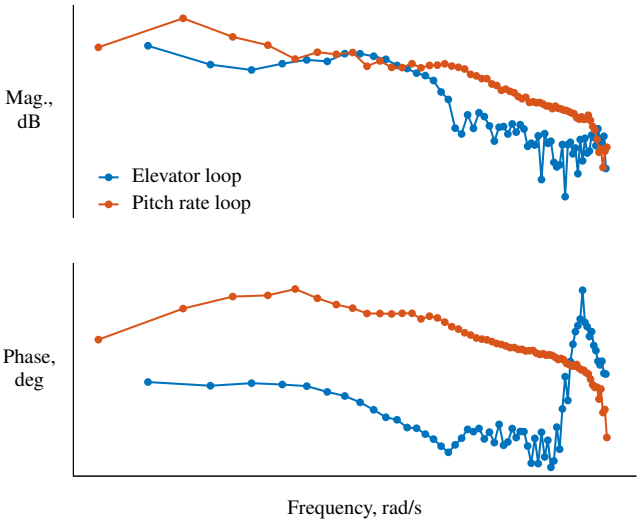

Fig. 5. X-56A longitudinal broken-loop frequency responses.

5.4 Bare-Airframe Parameter Estimation

Throughout the flights, multisines were injected at the actuator inputs ($\mathbf{r}_{ac}$ in Fig. 1) to estimate frequency responses for the bare-airframe dynamics, from which parametric state-space models were identified.

Figure 6 shows results from a longitudinal maneuver from Flight 11. Five multisines were added to the control surface commands as symmetric pairs and excited the longitudinal

dynamics. Bode plots for three of those surfaces are shown in Fig. 6. The dots are the estimated frequency response data and the lines are fits using a parametric model using these and other data. Estimated stability and control derivatives matched well to estimates obtained using other methods, as shown in Grauer and Boucher (2020b).

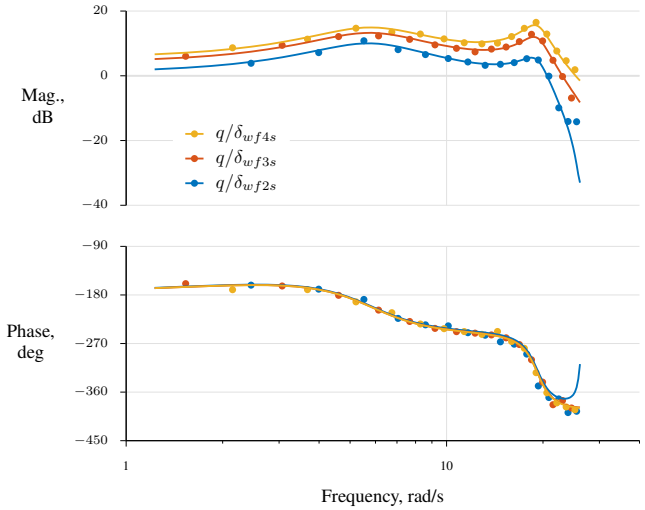

Fig. 6. X-56A longitudinal bare-airframe frequency response data (dots) and fitted models (lines).

6. CONCLUSIONS

Methods for frequency response estimation developed and used at NASA are summarized with flight test examples for the X-56A aeroelastic demonstrator. Using orthogonal phase-optimized multisine excitations enables the simultaneous identification of multiple control loops from multiple inputs using relatively simple computations that can be performed in real time. This has led to efficient flight tests and improved safety while reducing time and costs.

ACKNOWLEDGEMENTS

The efforts of the X-56A team at NASA Armstrong Flight Research Center are gratefully acknowledged. Technical discussions with Matthew Boucher and Jeffrey Ouellette are acknowledged and appreciated. Matthew Boucher designed the multisines used for Fig. 5.

REFERENCES

Baumann, E. (2007). Tailored excitation for frequency response measurement applied to the x-43a flight vehicle. Technical Report TP-2007-214609, NASA.

Bendat, J. and Piersol, A. (1986). *Random Data: Analysis and Measurement Procedures*. John Wiley & Sons, 2nd edition.

Berger, T., Tischler, M., Knapp, M., and Lopez, M. (2018). Identification of multi-input systems in the presence of highly correlated inputs. *Journal of Guidance, Control, and Dynamics*, 41(10), 2247–2257.

Bosworth, J. and Burken, J. (1997). Tailored excitation for multivariable stability-margin measurement applied to the X-31A nonlinear simulation. Technical Report TM-113085, NASA.

Bosworth, J. and Stachowiak, S. (2005). Real-time stability margin measurements for X-38 robustness analysis. Technical Report TP-2005-212856, NASA.

Bosworth, J. and West, J. (1986). Real-time open-loop frequency response analysis of flight test data. Number 86-9738 in AIAA Flight Testing Conference.

Brandon, J., Derry, S., Heim, E., Hueschen, R., and Bacon, B. (2008). Ares I-X stability and control flight test: Analysis and plans. Number 2008-7807 in AIAA Space Conference.

Grauer, J. (2018). Dynamic modeling using output-error parameter estimation based on frequency responses estimated with multisine inputs. Technical Report TP-2018-220108, NASA.

Grauer, J. (2022). Frequency response estimation for multiple control loops using orthogonal phase-optimized multisine inputs. *Processes*, 1–25 (submitted).

Grauer, J. and Boucher, M. (2020a). Aircraft system identification from multisine inputs and frequency responses. *Journal of Guidance, Control, and Dynamics*, 43(12), 2391–2398.

Grauer, J. and Boucher, M. (2020b). Real-time estimation of bare-airframe frequency responses from closed-loop data and multisine inputs. *Journal of Guidance, Control, and Dynamics*, 43(2), 288–298.

Grauer, J. and Morelli, E. (2014). Method for real-time frequency response and uncertainty estimation. *Journal of Guidance, Control, and Dynamics*, 37(1), 336–343.

Holzel, M. and Morelli, E. (2011). Real-time frequency response estimation from flight data. Number 2011-6358 in AIAA Atmospheric Flight Mechanics Conference.

Ljung, L. (1999). *System Identification: Theory for the User*. Prentice Hall, 2nd edition.

Milliken, W. (1947). Progress in dynamic stability and control research. *Journal of the Aeronautical Sciences*, 14(9), 493–519.

Morelli, E. (2002). System IDentification Programs for AirCraft (SIDPAC), ver. 4.1. NASA Software Catalog, `https://software.nasa.gov/software/LAR-16100-1`. Accessed January 2022.

Morelli, E. (2012). Flight test maneuvers for efficient aerodynamic modeling. *Journal of Aircraft*, 49(6), 1857–1867.

Morelli, E. and Grauer, J. (2020). Practical aspects of frequency-domain approaches for aircraft system identification. *Journal of Aircraft*, 57(2), 268–291.

Morelli, E. and Klein, V. (2005). Application of system identification to aircraft at NASA Langley Research Center. *Journal of Aircraft*, 42(1), 12–25.

Morelli, E. and Klein, V. (2016). *Aircraft System Identification: Theory and Practice*. Sunflyte Enterprises, 2nd edition.

Regan, C. (2008). In-flight stability analysis of the X-48B aircraft. Number 2008-6571 in AIAA Atmospheric Flight Mechanics Conference.

Ryan, J., Bosworth, J., Burken, J., and Suh, P. (2014). Current and future research in active control of lightweight, flexible structures using the X-56 aircraft. Number 2014-0597 in AIAA SciTech Forum.

Seamans, R., Blasingame, B., and Clementson, G. (1950). The pulse method for the determination of aircraft dynamic performance. *Journal of the Aeronautical Sciences*, 17(1), 22–38.

Tischler, M. and Remple, R. (2012). *Aircraft and Rotorcraft System Identification: Engineering Methods with Flight Test Examples*. AIAA, 2nd edition.